Mon. Not. R. Astron. Soc. **000**, 000–000 (0000) Printed 5 February 2008 (MN LATEX style file v1.4)

UBVRI CCD photometry of the old open cluster NGC 6253⋆

A. Bragaglia[1], G. Tessicini[1], M. Tosi[1], G. Marconi[2], U. Munari[3]

[1] *Osservatorio Astronomico di Bologna, Italy, e-mail angela@astbo3.bo.astro.it, loiano@astbo3.bo.astro.it, tosi@astbo3.bo.astro.it,*

[2] *Osservatorio Astronomico di Monte Porzio, Italy, e-mail marconi@coma.mporzio.astro.it*

[3] *Osservatorio Astrofisico di Asiago, Italy, e-mail munari@astrpd.pd.astro.it*

ABSTRACT

We present UBVRI photometry for the old open cluster NGC 6253. From comparison of the observed colour-magnitude diagrams with simulations based on stellar evolutionary models we derive in a self consistent way reddening, distance, and age of the cluster: E(B−V)= 0.23–0.32, (m-M)$_0$ = 10.9±0.1, metallicity roughly double than solar, and age $\simeq$ 3 Gyr. The cluster has a binary sequence, discernible even through the field contamination, suggesting that about 1/3 of the cluster members belong to binary, or multiple, systems.

Key words: Hertzsprung-Russel (HR) diagram – open clusters and associations: individual: NGC 6253 – Age – Metallicity

1 INTRODUCTION

Open clusters are a key probe of the chemical evolution and dynamics of the Galaxy (e.g., Janes 1979, Panagia and Tosi 1981, Friel and Janes 1993, Tosi 1996) and the interactions between thin and thick disks (e.g., Sandage 1988), since they provide more reliable information on the average stellar ages and radial velocities at different galactic radii (e.g., Janes and Phelps 1995) than field stars. They are among the very few galactic objects for which meaningful distances can be derived over a large range, which makes them an essential tool to constrain galactic evolution theories. However, to appropriately exploit the potentialities offered by open clusters, homogeneous and high quality observational material, as well as accurate data treatments, are mandatory to avoid misleading effects (e.g, Carraro and Chiosi 1994, Friel 1995).

We have undertaken a project aimed to secure photometric observations of the required accuracy for a well chosen sample of open clusters mapping a grid of ages, metallicities and galactocentric distances. The goal is to expand the number of clusters for which good quality photometric data are available, to constrain current theories on the dynamics, structure and chemical evolution of the Galaxy. Relevant cluster parameters are usually obtained by fitting theoretical isochrones to the observed color-magnitude diagrams (CMDs). We follow a different approach, namely the comparison of observed CMDs with synthetic ones generated by numerical codes based on stellar evolutionary tracks (Tosi et al. 1991), which we have found to be quite more powerful in investigations both of galactic clusters (Bonifazi et al. 1990) and of nearby irregular galaxies (Marconi et al. 1995).

In this paper we examine NGC 6253, an old open cluster so far scantly studied, located toward the galactic center ($\alpha_{1950} = 16^h55.1^m, \delta_{1950} = -52°38'$; $l^{II} = 336°$, $b^{II} = -6°$). Our results on Collinder 261 (age $\geq 7 \times 10^9$ yrs and solar metallicity) have been presented by Gozzoli et al. (1996), while studies of NGC 2506 and NGC 6603 are in progress.

In section 2 we describe the observations and data analysis; in Section 3 we present the derived CMDs involving U,B,V,R,I filters and discuss the problem of back/foreground contamination and the presence of a conspicuous population of binary stars. Section 4 will be devoted to the comparison with synthetic CMDs and the derivation of metallicity, age, distance and reddening, and the findings will be discussed in Section 5.

2 OBSERVATION AND DATA REDUCTIONS

We have observed NGC 6253 at the Danish 1.54m telescope located in La Silla, Chile. The CCD mounted in direct imaging was a Tek 1000×1000, with a pixel scale of 0.377 arcsec/pixel and a total field of 6.8×6.8 arcmin. We observed two slightly overlapping fields, one centered at the cluster coordinates, and the other just North of it, intended as external field. Standard CCD fields (PG1323-086, PG1633+099, SA110, Mark A, T Phe; Landolt 1992) containing a total of 18 standards both blue and red were also acquired, as was the usual set of bias, dark exposures, and sky flats. Exposures were taken in the Johnson-Cousins U,B,V,R,I filters, both very short ($\sim$ 10 seconds) to avoid saturation at the

⋆ Based on observations made at ESO telescopes, La Silla, Chile

Figure 1. Map of the observed region of NGC 6253; North is up and East left, and the field of view is about 7×7 arcmin. This map derives from our photometry, so it may be incomplete (e.g., there is a very bright field star at ∼ 950, 270, not visible here). Also indicated are the four stars whose pixel and absolute coordinates are given in Table 2.

Table 1. Journal of observations. Exposure times are given is seconds.

Field	Date	U	B	V	R	I
Central	Jul 11-18, 1993	900,900,120,40	900,900,30	600,600,300, 60,10	600,120,120, 30,10,5	600,600,300,180, 60,30,30,5
North	Jul 11-18, 1993		60	30		30

bright end, and longer to reach deep on the main sequence. Table 1 gives a journal of the observations and the exposure times for all filters, while Figure 1 shows the central field here analysed. Table 2 lists the X, Y coordinates in pixels of four stars, and their equatorial coordinates, for possible conversion. The celestial coordinates were found identifying the stars in the Digitized Sky Survey† images distributed on CD-ROM. Precision is about 1 arcsec, both in right ascension and declination.

All the reductions have been performed in the IRAF‡ environment, using the DAOPHOT-II routines (Stetson 1987, 1992) in a standard way. Stars have been found in the deepest V frame, then every other frame has been aligned

† Digitalization operated at STScI, on material from the UK Schmidt telescope, operated by the Royal Observatory Edinburgh and the Anglo-Australian Observatory

‡ IRAF is distributed by National Optical Astronomy Observatories, which is operated by the Association of Universities for Research in Astronomy Inc., under contract to the National Science Foundation.

Figure 2. Calibration relations: residuals of the fits for the various photometric bands.

Table 2. Pixel and equatorial coordinates for the four reference stars indicated in Figure 1.

n	Star N.	X,Y (pixel)	α, δ (2000.0)
1	2008	817.16, 411.41	16 58 49.90, −52 42 59.05
2	3595	429.94, 722.28	16 59 05.75, −52 41 05.35
3	890	133.36, 191.01	16 59 18.04, −52 44 23.63
4	2726	358.67, 552.43	16 59 08.58, −52 42 08.05

to it, and a single list of objects was used to derive instrumental magnitudes using PSF fitting. We then applied an aperture correction to the instrumental magnitudes, empirically derived from 10-20 isolated stars.

Standard stars fields were analysed using aperture photometry. The calibration equations were derived using the extinction coefficients for La Silla taken from the database maintained by J. Burki (Geneva Obs.) on the ESO/La Silla archive, accessible through `www` (http://archhttp.hq.eso.org), and are the following:

Table 3. Completeness of our measurements for the B,V,R,I filters: this is the average of 15 experiments. Smaller prints indicate that the errors were higher than 0.1 mag.

mag	% B	% V	% R	% I
12	100	100	100	100
13	100	100	100	100
14	100	100	100	100
15	100	100	100	100
16	100	100	100	100
17	100	100	100	100
18	100	100	100	91
19	100	100	92	76
20	100	89	71	63
20.5	92	76	32	33
21	80	56	13	14
21.5	68	28	3	5
22	50	9	2	1
22.5	31	1		
23	13			
23.5	2			
24	1			

$$U = u + 0.104(\pm0.033) \cdot (u - v) - 5.219(\pm0.012)$$

$$B = b + 0.194(\pm0.024) \cdot (b - v) - 4.640(\pm0.010)$$

$$V = v + 0.016(\pm0.008) \cdot (b - v) - 4.371(\pm0.007)$$

$$R = r + 0.051(\pm0.016) \cdot (v - r) - 4.476(\pm0.009)$$

$$I = i - 0.021(\pm0.013) \cdot (v - i) - 2.701(\pm0.008)$$

where *u, b, v, r, i* are instrumental magnitudes, while U, B, V, R, I are the corresponding Johnson - Cousins magnitudes.

In the central field a total of 5107 objects were detected, but we retained only those with internal photometric error given by DAOPHOT $\sigma \leq 0.1$ mag in all bands. We then calibrated each frame/filter and later averaged over the same filter to obtain the mean magnitude in each band. For the shorter exposures, only the brightest bins were considered in the average process. Furthermore we visually inspected and corrected all cases where the to-be-averaged values differed by more than 0.15 mag: in almost all cases this happened for very faint objects.

As final result, about 4200 stars have magnitudes in all the four B,V,R,I bands. The U exposures were much shallower and only about 1450 stars have been detected in all the 5 filters. A table with the 5 magnitudes and positions in pixel for all objects is available electronically from the first author.

To estimate the completeness degree of our measurements we added artificial stars at random positions (using the DAOPHOT routine Addstar) to the deepest frame in each filter; we added about 10% of stars in each magnitude bin, distributed in colours as the real ones. The frame was then reduced again, using exactly the same procedure and the same parameters and PSF as before, and we counted the recovered artificial stars for each bin. The experiment was repeated 15 times per filter and in Table 3 we present the average results, except those for the U band, where completeness reflects the much less severe crowding conditions with comparison to the other filters and is therefore misleading.

Figure 3. CMDs of NGC 6253: a) U *vs* U–B; b) V *vs* B–V; c) V *vs* V–R; V *vs* V–I. Only stars with internal errors $\leq$ 0.1 mag were considered in the average.

3 THE COLOUR MAGNITUDE DIAGRAMS

In Figure 3 and 4 we present the CMDs for NGC 6253 obtained from our reductions of the central field: in Figure 3a,b,c,d we show the "classical" CMDs using the 5 filters, while Figure 4a,b,c is dedicated to the U band and the red filters. Even if the field stars dominate in number, the cluster main sequence (MS) is easily located in all diagrams, and is well defined for at least 5 magnitudes fainter than the Turn-Off (TO). The upper MS terminates with a "hook" and it shows a clear gap just below it. The TO (the bluest point of the hook) is located at V$\simeq$14.7, B–V$\simeq$0.75. The TO morphology is probably complicated by the presence of a sequence of binary stars (see later) which converges there in the single-stars MS. Well defined subgiant and red giant branches are visible, as is a red clump at V=12.7, which we interpret as the locus of core-He burning stars. The magnitude distance between TO and red clump is δV=2.0. Also, there is a well populated sample of blue stragglers.

NGC 6325 has metallicity at the very least solar (see Section 4), and metal rich globular clusters (e.g. Ortolani, Bica & Barbuy 1993) often show anomalously extended red giant branches due to large blanketing effects. This phenomenon has been attributed to some open clusters as well, like NGC 6791 (Garnavich et al. 1994) which is very old and slightly more metal rich than the sun, and Cr 261 (Mazur et al. 1995) which is very old but with a metallicity probably lower than solar (Friel et al. 1995, Gozzoli et al. 1996).

Figure 4. Further CMDs of NGC 6253 involving the U band: a) U *vs* U–V; b) U *vs* U–R; c) U *vs* U–I. Note the presence of a binary sequence above the cluster MS.

Despite its larger metallicity, our data on NGC 6253 do not show such extension and turn down of the RGB, unless one pretends to define it through the two redder bright stars of the CMDs in Figure 3. We do not consider this lack as surprising, though, due to the relatively small number of red giants.

From the structure of the cluster CMD we can already infer that it is old, but not older than some Gyr, because of the presence of the MS gap and hooked termination. We will find (see next Section) an age of about 3 Gyr. No comparison with previous results is possible, since this is the first study of the cluster.

3.1 The Lower Main Sequence

Note that the cluster MS looks increasingly less populated going towards fainter luminosities: there seems to be a flattening of the present mass function for low-mass stars. This of course reflects on the luminosity function and the comparison with synthetic diagrams (see next Section). This flattening is not unusual or unexpected in old open clusters (see the review by Friel 1995) and has already been noticed e.g., in NGC 752 and M 67 (Francic 1989, Fan et al. 1996), NGC 2506 (Scalo 1986), King 2 (Aparicio et al. 1990), and as an extreme case in NGC 3680 (Nordstrom et al. 1995). Also in NGC 2243 (Bonifazi et al. 1990), a cluster very similar to NGC 6253, this fading of the MS is noticeable, even if not explicitly analysed by the authors. A likely explanation in old clusters is dynamical relaxation with ensuing mass segregation of higher mass stars towards the central parts and evaporation of lower mass stars (also favoured by tidal stripping due to encounters with massive clouds). This effect has been noticed also in younger clusters, like NGC 225 (age 10^8 yr, Lattanzi et al. 1991), which has photometry, astrometry and spectroscopy of good quality, and even in very young clusters (age $\sim 10^6$ yr, e.g. NGC 2362, Wilner & Lada 1991), where relaxation should not have had time yet to work out its effects.

Figure 5. Fore/background contamination as shown by the V *vs* B-V CMD of the control field.

Recently a similar fading of the MS has been found also for a globular cluster: Paresce, De Marchi & Romaniello (1995) presented HST data for NGC 6397, where the lower

Figure 6. CMDs of NGC 6253 at different radii from the centre: the cluster features, and most conspicuously the subgiant and red giant branches and the red clump, are well defined in all three panels

MS, close to the H burning limit, is much less populated than expected. In this case evaporation of low mass stars from the cluster is the favoured explanation, since the relaxation time for the cluster is small compared to its age, and the system is close to the Galactic plane, even if a peculiar IMF is not excluded by the authors.

3.2 Field decontamination

The true cluster diameter is larger than that found in the literature (5 arcmin, Lang 1992), and one has to move 8 arcmin from the cluster centre to find a legitimate external field. Figure 5 presents the CMD for the external field stars, extracted from the Northern frame. Given the exposure times used, we did not saturate objects in this external field, so the lack of stars brighter than about V=14.7 is real. The field comes from a mixed population, since it exhibits both a blue main sequence extending to about V=15, and an older/farther main sequence with TO at V=19, B–V=0.9 and relative subgiant/red giant branch. Given the galactic location of NGC 6253 and that resulting for this old component by extrapolating on the cluster line of sight, we interpret it as the old population across and beyond the Sagittarius spiral arm.

Fore/background contamination is severe, but not irrecoverable since cluster and field stars can be well distinguished in the CMDs involving the bluer bands: the separation is especially noticeable in the U *vs* U–V, U–R, U–I planes (see Figure 4). Unfortunately, the U band is also that where less stars were detected, so we decided to attempt a cluster-field segregation in the classical V *vs* B–V diagram; there too the separation is apparent, and we think we can isolate *bona fide* field stars with reasonable confidence, at least on the blue side of the MS. Results of our classification are shown in Figure 8, where the heavier symbols indicate probable cluster members, and the lighter ones probable field stars. All the red giants have been assigned to the cluster, due to their absence in the external field.

Besides, the cluster features are well distinguishable in all panels of Figure 6, where we show the run of the V *vs* B–V CMD with different radial distances from the cluster centre (taken by visual inspection of the map to be at pixel 400,500). The number of field stars appears to decrease from panel a) to c) more dramatically than that of the cluster members, while the subgiant and red giant branches and even the red clump remain well delineated: we interpret this as further confirmation of their being cluster members.

3.3 Binary stars

Presence of binary stars in open clusters is not an uncommon phenomenon: most open clusters show in fact indications of a sizeable binary population. Mermilliod & Mayor (1989, 1990) during a Coravel radial velocity survey of 10 clusters as old or older than the Hyades, found a percentage of spectroscopic binaries around 30 % in all of them. As examples of photometric detections, Aparicio et al. (1990), from the scatter of the main sequence, found that about 50% of the stars in King 2 are binaries. Very well defined sequences are visible in NGC 2243, where at least 30% of the members are binary systems (Bonifazi et al. 1990), in M 67 (Montgomery et al. 1993 estimate $\gtrsim$ 38% of binaries, and Fan et al. 1996 reach 50%) or in NGC 2420 (Anthony-Twarog et al. 1990 derive about 50% of binaries).

The case of NGC 6253 is not as well defined as these; we can clearly see (Figures 3, 4 and 6) a secondary sequence of stars right above the cluster MS, at a distance of about 0.7 mag, just what we would expect in presence of a significant

Figure 7. Top panels: Histograms of the colour distribution in U–R relative to the MS ridge line for magnitudes in the range U=17-20. The MS peak is at 0 by definition, and the position of the secondary peak expected in each magnitude bin in presence of binary systems is indicated by an arrow. Bottom panel: Histograms of the U-magnitude difference of all stars relative to the MS ridge line. The arrow indicates the expected position of equal mass binaries.

fraction of binary systems. The evidence is more convincing when looking at CMDs built using the U and red filters (Figure 4), since the separation between the MS and field stars is larger, and the binary sequence is better discernible. Unfortunately, the field population smears out the MS and binary sequence distributions. In order to somewhat quantify the visual impression of a secondary sequence, we have built the histograms of the colour difference (e.g. in U–R, see top panels in Figure 7) between each star and the MS ridge line (interpolated by eye) at different magnitude levels. In all panels, except the very faintest where any feature is wiped out by the errors, a small secondary peak to the right of the MS one is visible. Despite its small size, this peak provides strong support to the binary stars hypothesis, since it appears almost exactly at the colour (indicated by an arrow) where the peak of equal mass binaries is predicted to occur. Notice that this does not mean that the binaries have equal mass components: as discussed in the pioneering work by Maeder (1974) and most recently by Fan et al. (1996), binary components with mass ratios q lower than 0.5 are indiscernible from the single stars MS, because photometric errors are larger than their colour and magnitude difference, whereas binaries with $0.5 \lesssim q \lesssim 0.9$ spread out between the single star MS and the equal mass binary ridge where the remaining binaries concentrate. In fact, both the appearance of the CMD and the histograms derived for NGC 6253, look very much the same as those shown by Fan et al. (1996) for M 67, where the fraction of binaries is estimated around 50% and their mass ratios randomly distributed between 0 and 1.

An alternative test is to look at the distributions of magnitude differences between stars and the MS ridge line at each colour, since it should also present a secondary peak due to binaries (see e.g. Montgomery et al. 1993 for M 67). The results for our cluster are not as conclusive as theirs, given the larger field contamination. We have computed the magnitude differences in the U, U–R CMD, and their histogram is shown in the lower panel of Figure 7, with an arrow indicating the predicted location of objects 0.75 mag brighter than the MS: there is indeed a hint of secondary peak in that position, but definitely not significant.

As it is, we cannot derive a precise figure for the binary fraction, since we are plagued by field contamination. Taking into account that the number of stars in the secondary peak of Figure 7 histograms ranges between 0.14 and 0.27 times the total number of stars falling in both the primary and the secondary peaks, the apparent fraction of binary systems in NGC 6253 is approximately 20%. Due to the various effects discussed by Maeder (1974) and Fan et al. (1996), this presumably corresponds to a larger actual percentage of binaries.

An alternative explanation suggested by some authors for the MS skewness is differential extinction (due e.g. to a feeble dust lane, see Lattanzi et al. 1991 for NGC 225). In the case of NGC 6253, we reject this hypothesis, because the stars on the right of the MS have galactic locations uniformly distributed within the cluster, and in these conditions differential reddening should not create a second sequence clearly separated from the first one as in Figure 7 but rather a general spread of the whole MS.

4 CLUSTER PARAMETERS

We have applied to NGC 6253 the approach amply described by Tosi et al. (1991), and already employed for two other old open clusters (Bonifazi et al. 1990; Gozzoli et al. 1996). Briefly, this method represents an improvement of the classical isochrone fitting, allowing the simultaneous derivation of age, reddening and distance modulus, with the advantage of checking the relative number of stars in the various evolutionary phases. The observed CMDs of the cluster are compared with synthetic CMDs resulting from Monte Carlo simulations of a system containing the same number of stars above the same limiting magnitude, and with the same photometric errors and incompleteness factors in each

Figure 9. Synthetic CMDs derived from the FRANEC stellar evolutionary tracks. Panels (a) and (b) adopt Z=0.01, τ=2.5 Gyr, (m-M)$_0$=10.9 and E(B−V)=0.43; panels (c) and (d) Z=0.02, τ=3 Gyr, (m-M)$_0$=10.8 and E(B−V)=0.33.

Figure 8. CMD of NGC 6253 for the objects with $\sigma \leq 0.1$. Probable cluster members are indicated by filled circles, probable field stars by dots (see text for details).

magnitude bin as observed in the actual cluster. For each assumed evolution model, the resulting synthetic CMD is translated into the empirical one by finding the values of reddening and distance modulus providing the best agreement with the observed stellar distribution, and thus providing in turn metallicity, age, reddening and distance modulus at the same time. The resulting set of values, however, is not unique, because different stellar evolution models may lead to quite different solutions, as shown for instance by Gozzoli et al. (1996) for Cr 261. For this reason, we have derived the cluster parameters with three different data bases of stellar evolutionary tracks, and evaluated both the best parameter values and the corresponding theoretical uncertainties.

The synthetic diagrams simulated for NGC 6253 are based on homogeneous sets of stellar evolution models computed for several initial metallicities: a) the tracks with classical mixing length treatment of the convective zones computed by the Frascati-Teramo group (hereinafter FRANEC), b) the tracks with overshooting from convective cores computed by the Geneva group (hereinafter GENEVA), c) the tracks with overshooting from convective cores by the Padova group (hereinafter BBC). We have not used the tracks by D'Antona et al. (1992, hereinafter CM), applied to Cr 261, because they are available only for stellar masses smaller than those describing the upper CMD of NGC 6253.

Within the framework of each group of stellar models, we have performed several simulations for any reasonable combination of age, reddening and distance modulus, all of which have been compared with the empirical CMD and luminosity functions of NGC 6253. We describe below only the most significant cases, selected on the basis of these comparisons.

Since the synthetic CMDs obviously apply only to cluster members, we have selected from the stars detected in the field of NGC 6253 and with photometric error smaller than 0.1 mag in all bands but U, only those that can be taken as probable members (see section 3.1). This selection restricts the sample to 641 objects out of 4200; all the others are presumably back/foreground stars. The supposed members are represented in Figure 8 with the larger symbols, the other objects with the small ones. The synthetic diagrams discussed below therefore assume the cluster to be populated by 641 stars.

We have shown in the previous section that this cluster is probably populated by a significant fraction of binary systems. To further check this point, we have performed our Monte Carlo simulations either assuming that all the cluster members are single stars or that a varying fraction of them are binaries. In the latter cases, for each binary system we have assumed a secondary/primary mass ratio randomly extracted from a flat distribution. Colour and magnitude of each system are assigned according to the mass ratio and following Maeder's (1974) prescriptions. This implies, for instance, that a system formed of equal mass stars has the same B–V as each of the two stars and a magnitude corresponding to double brightness (i.e. 0.75 mag brighter). A system with mass ratio 0.8 shows a B–V 0.04 mag redder, and a V 0.35 mag brighter, than the primary star; systems with $q \leq 0.6$ have in practice the same colour and magnitude of the primary star.

4.1 Results with FRANEC stellar models

FRANEC sets of models follow the evolution of stars between 0.6 and 1 $M_\odot$ in the central hydrogen and helium burning phases and the evolution of stars between 1 and 9 $M_\odot$ up to the onset of thermal pulses on the asymptotic giant branch. Of the available sets with different initial helium and metal abundances, we have used for NGC 6253 those with Y and Z equal to (0.27, 0.01), (0.27, 0.02), (Castellani et al. 1993).§

Figure 9 (c) shows one of the best synthetic diagrams obtained with Z=0.02 for a full population of single stars. The adopted parameters are: τ=3 Gyr, E(B–V)=0.33, $(m\text{-}M)_0$=10.8. The shapes and locations of the MS and TO predicted by the single star models are correct, including the hook, the gap and the relative number of stars in the various phases. However, all the stars on the red side of the MS are missing. This inconsistency can be easily overcome by including a proper fraction of binary systems in our simulations. In fact, panel (d) shows the same CMD as panel (c), but for a population with 30% binaries and random q, and reproduces quite well all the observed features of the MS and TO regions. We have performed similar simulations with other percentages of binary systems and found that lower fractions do not fill the MS enough, whereas higher percentages bring too many objects above the subgiant branch of single stars.

A striking feature of all the performed simulations, for this as well as for all the other sets of stellar models, is that, if we adopt the incompleteness factors of Table 3, empirically derived from the CCD frames, the resulting synthetic CMDs systematically overestimate the number of faint stars. This phenomenon is apparent in the luminosity functions (LF) of Figure 10, where the dots correspond to the observational data and the thick dashed curve to a model adopting the same parameters as above and the empirical incompleteness. In order to predict the right number of stars in the fainter bins (and consequently in the bright ones as well), one has to artificially alter the actual incompleteness factors below V=17. This discrepancy is not due to an underestimate of the incompleteness (we have performed the artificial star test 15 times obtaining always very similar results), but to a real decrease of the number of low mass stars, beyond any reasonable IMF. We are inclined to interpret this decrease in terms of evaporation from the cluster of the smallest stars, similar to what Fan et al. (1996) have found for M 67. In all the following we then show synthetic CMDs and LFs (thin curves) based on the modified incompleteness which allows to reproduce the faint end of the observational LF. The adopted incompleteness start to deviate from the em-

Figure 10. Luminosity function for the observed (dots) and synthetic (lines) stars members of NGC 6253. Top panel: LFs corresponding to the FRANEC models. The thick line results from adopting the actual incompleteness factors listed in Table 1, thin lines from that modified at the faint end (see text). The dotted line represents the Z=0.01 case of Figure 9 (b), the dashed line the Z=0.02 case of Figure 9 (d). Central panel: GENEVA models. The dotted line represents the Z=0.008 case of Figure 11 (b), the dashed line the Z=0.02 case of Figure 11 (d), and the solid line the Z=0.04 case of Figure 11 (f). Bottom panel: BBC models. The dashed line represents the Z=0.02 case of Figure 12 (b) and the solid line the Z=0.05 case of Figure 12 (d).

§ Note that these tracks have been computed with the LAOL Los Alamos opacities. According to the authors, the effect of using instead the most recent OPAL Livermore opacities corresponds only to assuming a slightly larger metallicity (Cassisi et al. 1993). Therefore, the metallicity of the FRANEC models mentioned above should actually be taken as about half of their nominal Z value.

pirical one below V=17, and becomes a factor of 5 more severe at V=21.

Finally, the model shown in Figures 9 (c) and (d) shows a subgiant branch more extended in colour than the actual branch of NGC 6253 and, as a consequence, a too red RGB. Binary stars obviously do not help in the RGB region, although the observed spread in the CMD distribution of the red giants (which, at this bright magnitudes, cannot be attributed to photometric errors) is probably due the binary stars effect. Due to the increased size of post-MS stars, such effect after the exhaustion of the central hydrogen is much more complicated than the simple shift in magnitude and colours assumed here; however, it is apparent that it cannot push the predicted distribution bluewards, as would be necessary to fit the data. A lower E(B–V) cannot be invoked to solve this discrepancy, because it would obviously improve the fitting of the red CMD region but worsen the blue region. We will see in the following that this discrepancy is probably a metallicity effect.

Figures 9 (a) and (b) show the best synthetic diagrams, with and without binaries, obtained with Z=0.01. The adopted parameters are: τ=2.5 Gyr, E(B–V)=0.43, $(m\text{-}M)_0$=10.9. As in the previous case, a 30% fraction of binary stars is required to properly reproduce the colour and magnitude extension of the MS, as well as the global LF (see dotted line in Figure 10). The synthetic subgiant branch shows a colour extension even larger than in the solar metallicity case and the RGB is too red.

To verify whether a larger metallicity could help to reproduce the observed cluster features, we have made some further simulations with the new tracks with Y=0.34 and Z=0.04 kindly made available by S. Cassisi and computed with the new OPAL opacities and a slightly different version of the FRANEC code (Bono et al. 1996 in preparation). This set is however not homogeneous to the other two, due to the different input physics, and this does not allow to use it fruitfully for our purposes.

4.2 Results with GENEVA stellar models

The stellar evolution tracks computed by the Geneva group take into account the possible overshooting of convective regions out of the edges defined by the classical mixing length theories. The models have been computed for the mass range 0.8 and 120 $M_\odot$ and several initial metallicities. For NGC 6253 we have tested the cases with initial Y and Z (0.26, 0.008), (0.30, 0.02) and (0.34, 0.04) presented by Schaerer et al. (1993b), Schaller et al. (1992) and Schaerer et al. (1993a), respectively. The low mass stellar models with solar metallicity are followed up to the early asymptotic giant branch phase (Charbonnel et al. 1996), the others only to the tip of the RGB, therefore only for the solar composition cases can our synthetic diagrams show the red clump corresponding to the central helium burning of low mass stars. The lack of stellar models for masses below 0.8 $M_\odot$ and for the clump makes the synthetic CMDs not completely comparable with that of NGC 6253, but the cluster parameters can be derived anyway.

Stellar tracks with lower initial metallicity have bluer MS and more extended subgiant branch. The first phenomenon implies that the corresponding synthetic diagrams require larger reddenings to fit the observed distribution. Combined with the larger colour extension of the subgiant branch, this however leads to quite red RGBs, so that, for all the performed simulations, the lower the initial metallicity, the redder the final RGB. As a consequence, models with Z=0.008 and Z=0.02 are not able to properly reproduce the empirical CMD of NCG 6253, whereas models with Z=0.04 are in agreement with the location of both the blue and the red stars.

Figure 11 (a) shows the best synthetic diagram obtained with Z=0.008 for a full population of single stars. The adopted parameters are: τ=2.5 Gyr, E(B–V)=0.46, $(m\text{-}M)_0$=10.9. The shapes and locations in the CMD of the MS and TO predicted by the single star models are correct, but all the stars on the red side of the MS are missing. Panel (b) shows the corresponding CMD for a population with 30% binaries. It is apparent from the shown CMDs that with this set of tracks, as well as with the other GENEVA sets, the inclusion of binary systems places too many bright stars right after the TO, due to the fact that the timescale of this phase is longer in the GENEVA than in the FRANEC and BBC models. We have checked whether we could reduce the number of binary post-TO stars by reducing the fraction of multiple systems, but we have not reached satisfactory solutions. In fact, any decrease of the binary fraction has much more effect on the number of MS objects than on that of subgiants and we end up with a clear underestimate of the MS binaries while still having too many early subgiant binaries.

The red clump is absent because these stellar tracks do not reach that phase, and this absence is the reason for the slight underestimate of the number of bright stars apparent in the luminosity function (central panel in Figure 10). The lack of stellar tracks for M<0.8 $M_\odot$ is the cause the abrupt fall of these theoretical luminosity functions.

Figure 11 (c) and (d) show the best synthetic diagram obtained with Z=0.02 for a full population of single stars and for a population with 30% binaries, respectively. The adopted parameters are: τ=3 Gyr, E(B–V)=0.36, $(m\text{-}M)_0$=10.9. For this set of tracks the core He-burning phase has been computed and the corresponding red clump falls in the synthetic CMD at the same brightness (V$\simeq$12.7) as the observational one, but at redder colour (Δ(B–V)$\simeq$0.05). As for the Z=0.008 case, a lower reddening would not solve the problem, which is clearly a consequence of the intrinsic shape of the subgiant branch in these stellar models. As for the Z=0.008 case, 30% binaries provide too many bright subgiants.

Finally, Figure 11 (e) and (f) show the best synthetic diagram obtained with Z=0.04 adopting: τ=3 Gyr, E(B–V)=0.32, $(m\text{-}M)_0$=10.9. Again, as for Z=0.008, the red clump is absent from these stellar tracks. Aside from this point, both the synthetic CMD and LF reproduce quite well the various data features. The Geneva models therefore indicate that NGC 6253 has a metallicity double than solar.

4.3 Results with BBC stellar models

Also the stellar evolution tracks computed by the Padova group take overshooting from convective cores into account, although with a treatment different from that adopted by the Geneva group. They have been computed for masses between 0.5 and 120 $M_\odot$ and for several initial metallicities.

Figure 11. Synthetic CMDs derived from the GENEVA stellar evolutionary tracks. Panels (a) and (b) adopt Z=0.008, τ=2.5 Gyr, $(m\text{-}M)_0$=10.9 and E(B−V)=0.46; panels (c) and (d) Z=0.02, τ=3 Gyr, $(m\text{-}M)_0$=10.9 and E(B−V)=0.36; panels (e) and (f) Z=0.04, τ=3 Gyr, $(m\text{-}M)_0$=10.9 and E(B−V)=0.32.

Figure 12. Synthetic CMDs derived from the BBC stellar evolutionary tracks. Panels (a) and (b) adopt Z=0.02, τ=4 Gyr, $(m\text{-}M)_0$=10.7 and E(B−V)=0.30; panels (c) and (d) Z=0.05, τ=3 Gyr, $(m\text{-}M)_0$=11.0 and E(B−V)=0.23.

They reach the tip of the asymptotic giant branch or the ignition of the core C-O burning phase, depending on the initial stellar mass. For NGC 6253, we have tested the sets of tracks with Y and Z equal to (0.28, 0.008) by Alongi et al. (1993), (0.28, 0.02) by Bressan et al. (1994) and (0.352, 0.05) by Fagotto et al. (1994), available at the Strasbourg Data center.

As already found for the Geneva models, tracks with lower metallicity show bluer MS, larger colour extension of the subgiant branch, redder RGB. Therefore, models with Z=0.008 do not reproduce well the data and we do not show them here. Models with solar metallicity are not satisfactory either. Figures 12 (a) and (b) show the BBC synthetic CMDs with Z=0.02 in better agreement with the data, respectively without or with 30% binaries. They assume τ=4 Gyr, E(B−V)=0.3 and $(m\text{-}M)_0$=10.7. With the binaries included the simulation reproduces pretty well the MS and the TO stellar distribution both in the CMD and in the LF (Figure 10). The synthetic CMD shows too red colours for the giants, thus suggesting that NGC 6253 has a metallicity larger than solar.

Figure 12 (c) shows the BBC synthetic CMD in better agreement with the data. Figure 12 (d) shows the corresponding CMD with 30% of binary stars. They both assume large initial metallicity Z=0.05, τ=3 Gyr, E(B−V)=0.23 and $(m\text{-}M)_0$=11.0 and reproduce pretty well the MS and post-MS colours, luminosities and stellar distributions (see also the LF for the case with binaries in the bottom panel of Figure 10). With the Padova models we thus find, as with the Geneva ones, that NGC 6253 is metal rich and ∼3 Gyr old.

5 CONCLUSIONS

Open clusters are a class well suited to study the structural and evolutionary changes in our Galaxy. In spite of all the uncertainties in dating them, and of the fact that even the age ranking is not totally safe when simply taken from literature values, they provide ages more accurate than any other disk objects. Ideally one would like to determine ages consistently, fitting uniform sets of theoretical models to clusters whose metallicities and reddenings are well constrained by observations. This is a tough job, given the difficulties in obtaining precise enough photometry, and can be done only for a limited sample of clusters. Also, reddenings are usually very badly, if at all, known. Metallicities are in a better situation, since they have been measured for many clusters through narrow-band photometry or spectroscopy, both with low and high resolution (Friel 1995). Our method, with the advantage of determining at the same time age, distance, reddening and metallicity, can circumvent most of these problems and the main conclusions that can be derived are the following.

a) In the case of NGC 6253 we find that age and distance modulus are very tightly derived with the synthetic CMD method. In fact, the best reproduction of the observed cluster features is obtained assuming τ=3.0±0.5 Gyr and $(m\text{-}M)_0$=10.9±0.1, whatever the adopted class of stellar models; a striking agreement if we consider that different tracks can lead to rather different ages, as we found e.g. for NGC 2243 (Bonifazi et al. 1990) and Cr 261 (Gozzoli et al. 1996).

b) The reddening derived from our analysis of NGC 6253 is rather large, 0.23≤E(B–V)≤0.32, as expected from the galactic location of the cluster, which not only is toward the center, but falls on the Sagittarius spiral arm. The intrinsic differences between the various sets of adopted models are responsible for the uncertainty on the derived value. For any given metallicity, in fact, the GENEVA tracks are intrinsically hotter, and the BBC tracks cooler, than the others, thus implying systematically larger and smaller reddenings respectively.

c) A good qualitative agreement is achieved also in what concerns the cluster metallicity. Our method cannot provide the precise chemical abundance of the system, since it is limited at least by the restricted number of chemical composition cases of the available stellar tracks. However, it is apparent from the results presented in the previous section that NGC 6253 must have a metallicity roughly double than solar, since only in this case all the predicted locations in the CMD of MS, subgiant, RGB and red clump are simultaneously consistent with the empirical ones.

d) The lower main sequence shows clear indication that a fraction of low mass stars are missing, most probably due to evaporation through dynamical relaxation and mass segregation, as found in many other cases. No reasonable IMF could justify such an effect.

e) The cluster has a quite distinct secondary sequence, right above the single-star MS, attributable to binary systems. A sizeable population of binary stars ($\gtrsim$ 20 %) not at all unusual for open clusters, also leads to better agreement between the observed and the synthetic CMDs.

With this study we increase the number of well studied old open clusters, since, at an age of 3.0±0.5 Gyr, NGC 6253 falls in this small sample, whose properties like galactic locations, chemical abundances, ages can be used as reliable tracers of disk formation and evolution.

ACKNOWLEDGEMENTS

It's a pleasure to thank Laura Greggio for providing the numerical code which has been the bulk of the adopted procedure for CMD simulations, and P. Montegriffo whose programs we used to average and clean our measurements. We are indebted to F. Fusi Pecci for many useful suggestions. We also wish to thank P. Battinelli and L. Ciotti for interesting discussions about binaries and evaporations from the clusters. The FRANEC, GENEVA and BBC evolutionary tracks were kindly made available by their authors; in particular we are grateful to S. Cassisi and A. Chieffi for computing some tracks for us. This research has made use of the Simbad database, operated at CDS, Strasbourg, France.

REFERENCES

Alongi, M., Bertelli, G., Bressan, A., Chiosi, C., Fagotto, F., Greggio, L., Nasi, E. 1993, AAS, 97, 851

Anthony-Twarog, B.J., Kaluzny, J., Shara, M.M., Twarog, B.A. 1990, AJ, 99, 1504

Aparicio, A., Bertelli, G., Chiosi, C., Garcia-Pelayo, J.M 1990, A&A, 240, 262

Bonifazi, A., Fusi Pecci, F., Romeo, G., Tosi, M. 1990, MNRAS, 245, 15

Buonanno, R., Corsi, C.E., Fusi Pecci, F., Fahlman, G.G., Richer, H.B. 1994, ApJ, L121
Bressan, A., Fagotto, F., Bertelli, G., Chiosi, C. 1994, AAS 100, 647
Canuto, V., Mazzitelli, I. 1991, ApJ 370, 295
Carraro, G., Chiosi, C. 1994, AA, 287, 761
Caputo, F., Chieffi, A., Castellani, V., Callados, M., Martinez Roger, C, Paez, E. 1990, AJ, 99, 261
Cassisi, S., Castellani, V., Salaris, M., Straniero, O. 1994, A&A 282, 760
Castellani, V., Chieffi, A. & Straniero, O. 1993, ApJS 78, 517
Chaboyer, B., Demarque, P., Sarajedini, A. 1996, ApJ, 459, 558
Charbonnel, C., Meynet, G., Maeder, A., Schaerer, D. 1996, A&AS 115, 339
D'Antona, F., Mazzitelli, I., Gratton, R.G. 1992, AA 257, 539
Fagotto, F., Bressan, A., Bertelli, G., Chiosi, C. 1994, AAS 104, 365
Fan, X., et al. 1996, astro-ph/9604178 preprint
Francic, S.P. 1989, AJ, 98, 888
Friel, E.D. 1995, ARAA, 33, 381
Friel, E.D., Janes, K.A. 1993, AA, 267, 75
Friel, E.D., Janes, K.A., Hong, L., Lotz, J., Tavarez, M. 1995, in The Formation of the Milky Way, E.J.Alfaro and A.J.Delgado eds (CUP, UK), p.189
Garnavich P.M., VandenBerg D.A., Zurek D.R., Hesser, J.E. 1994 AJ, 107, 1097
Gozzoli, E., Tosi, M., Marconi, G., Bragaglia, A. 1996, MNRAS, in press
Janes, K.A. 1979, ApJS, 39, 135
Janes, K.A., Phelps, R.L. 1994, AJ, 108, 1773
Kaluzny, J., Krzeminski, W., Mazur, B. 1995, E.J.Alfaro and A.J.Delgado, eds, The Formation of the Milky Way, Cambridge University Press, UK, p.185
Landolt, A.U. 1992, AJ, 104, 347
Lang, K.R. 1992, Astrophysical Data: Planets ans Stars, Springer-Verlag, Berlin
Lattanzi, M.G., Massone, G., Munari, U. 1991, AJ, 102, 177
Maeder, A., 1974, A&A, 32, 177
Marconi, G., Tosi, M., Greggio, L., Focardi, P. 1995, AJ, 109, 173
Mazur, B., Krzeminski, W., Kaluzny, J. 1995, MNRAS, 273, 59
Mermilliod, J.C., Mayor, M. 1989, A&A, 219, 125
Mermilliod, J.C., Mayor, M. 1990, A&A, 237, 61
Montgomery, K.A., Marshall, L.A., Janes, K.A. 1993, AJ, 106, 181
Nordstrom, B., Andersen, J., Andersen, M.I, 1996, A&A, submitted
Ortolani S., Bica E., Barbuy B. 1993, A&A 267, 66
Panagia N., Tosi M. 1981, A&A, 96, 306
Paresce, F., De Marchi, G., Romaniello, M. 1995 ApJ, 440, 216
Phelps, R.L., Janes, K.A., Montgomery, K.A. 1994, AJ, 107, 1079
Phelps, R.L., Janes, K.A., Friel, E.D., Montgomery, K.A. 1995, E.J.Alfaro and A.J.Delgado, eds, The Formation of the Milky Way, Cambridge University Press, UK, p.187
Romeo G, Bonifazi A, Fusi Pecci F., Tosi M. 1989, MNRAS 240,459
Rufener, F. 1986, A&A, 165, 275
Sandage, A.R. 1988, A.G.D. Philip, L. Davis, eds, Calibration of stellar ages, (Schenectady USA), p.43
Scalo, J.M. 1986, Fund.Cosm.Phys. 11, 1
Schaerer, D., Charbonnel, C., Meynet, G., Maeder, A., Schaller, G. 1993a, A&AS 102, 339
Schaerer, D., Meynet, G., Maeder, A., Schaller, G. 1993b, A&AS 98, 523
Schaller, G., Schaerer, D., Meynet, G., Maeder, A., 1992, A&AS 96, 269
Stetson, P.B. 1987, PASP 99, 191
Stetson, P.B. 1992, User's Manual for DAOPHOT-II
Tosi, M. 1995, E.J.Alfaro and A.J.Delgado, eds, The Formation of the Milky Way, Cambridge University Press, UK, p.153
Tosi, M., Greggio, L., Marconi, G., Focardi, P. 1991, AJ, 102, 951
Wilner, D.J., Lada, C.J. 1991, AJ, 102, 1050

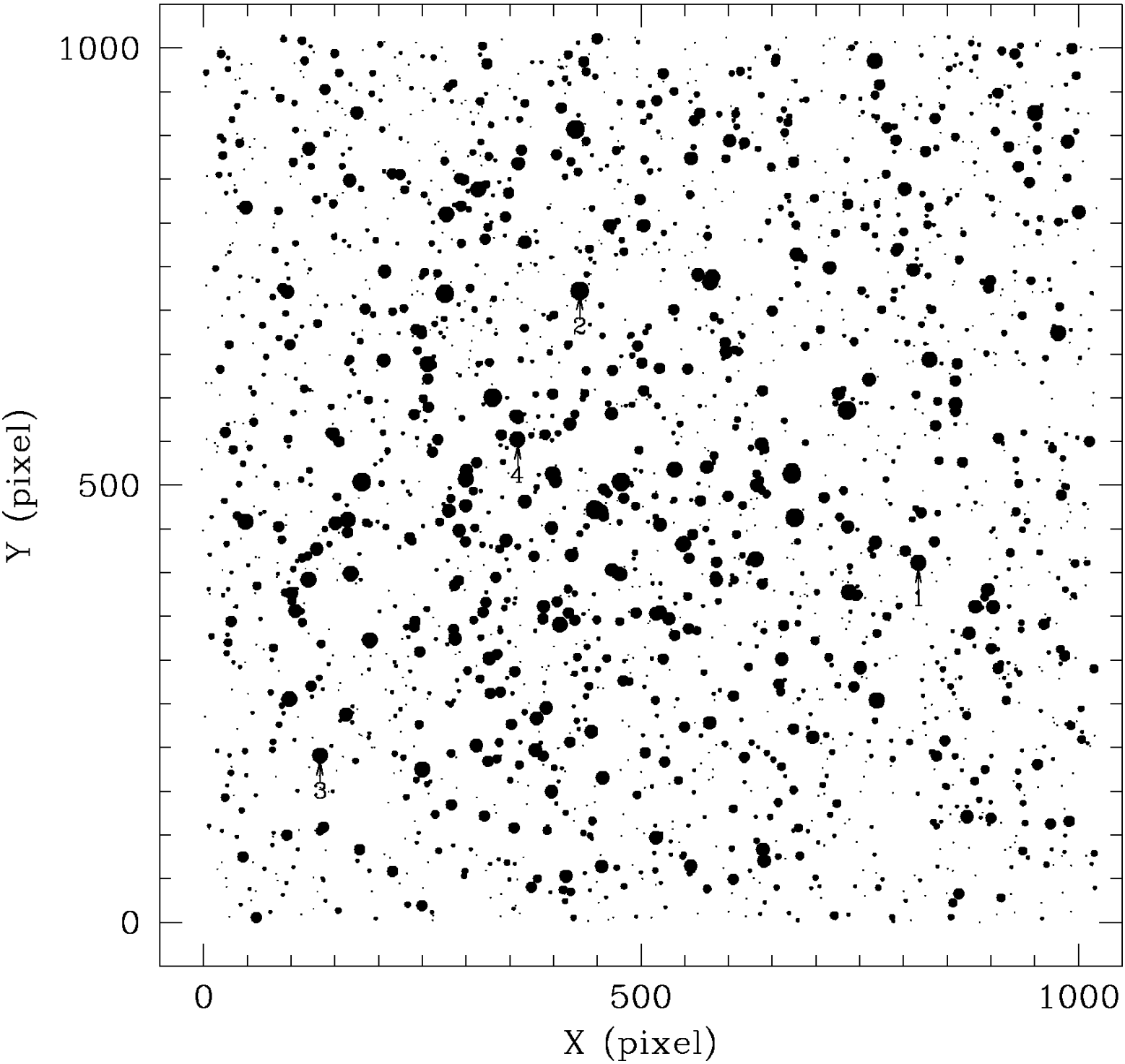
1000
500
0
Y (pixel)
0
500
1000
X (pixel)
1
2
3
4

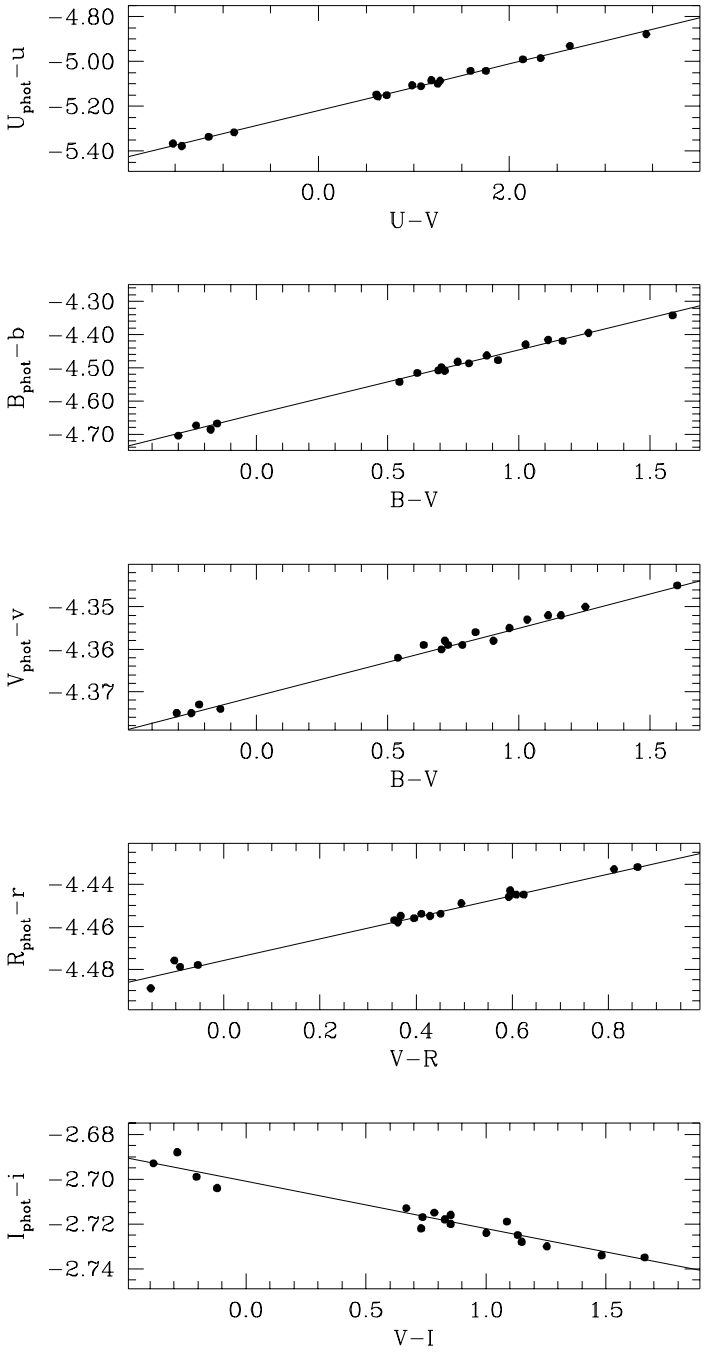
−4.80
−5.00
−5.20
−5.40
$U_{phot} - u$
0.0
2.0
U−V
−4.30
−4.40
−4.50
−4.60
−4.70
$B_{phot} - b$
0.0
0.5
1.0
1.5
B−V
−4.35
−4.36
−4.37
$V_{phot} - v$
0.0
0.5
1.0
1.5
B−V
−4.44
−4.46
−4.48
$R_{phot} - r$
0.0
0.2
0.4
0.6
0.8
V−R
−2.68
−2.70
−2.72
−2.74
$I_{phot} - i$
0.0
0.5
1.0
1.5
V−I

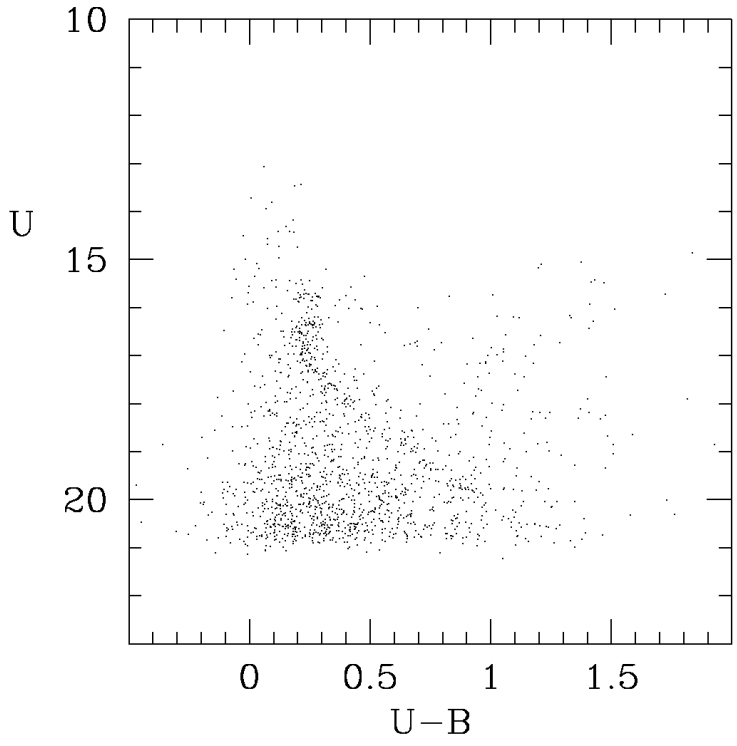
10
15
20
U
0
0.5
1
1.5
U−B

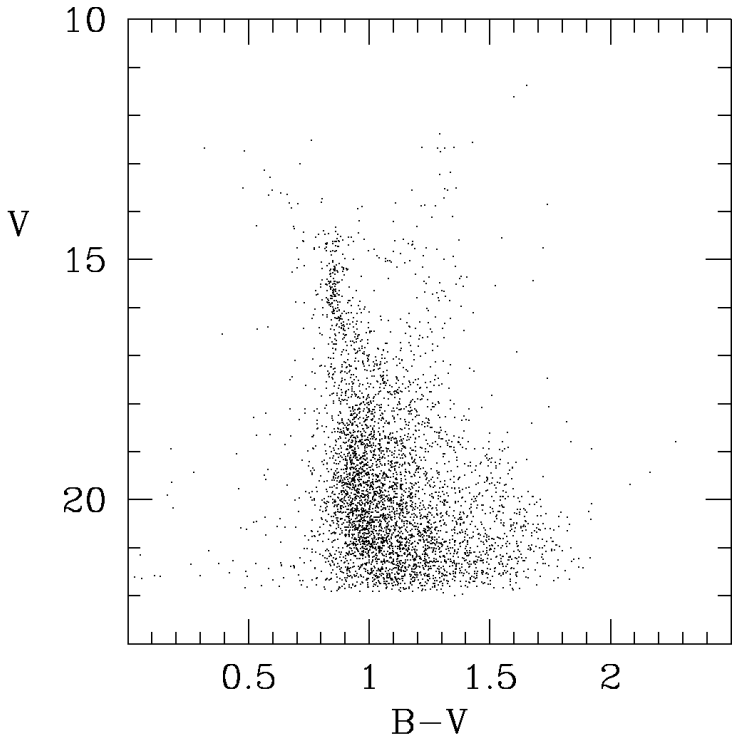
10
15
20
V
0.5
1
1.5
2
B−V

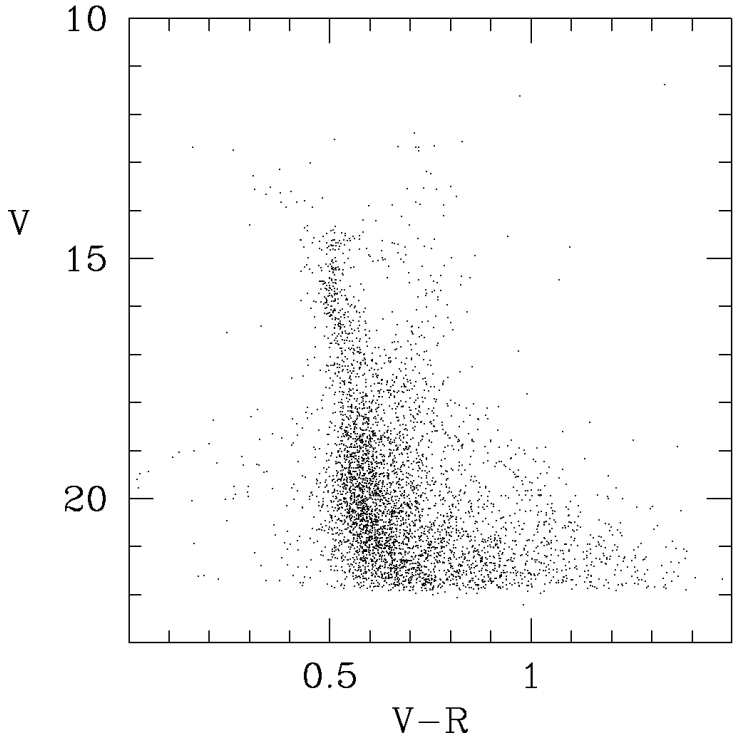
10
15
20
V
0.5
1
V−R

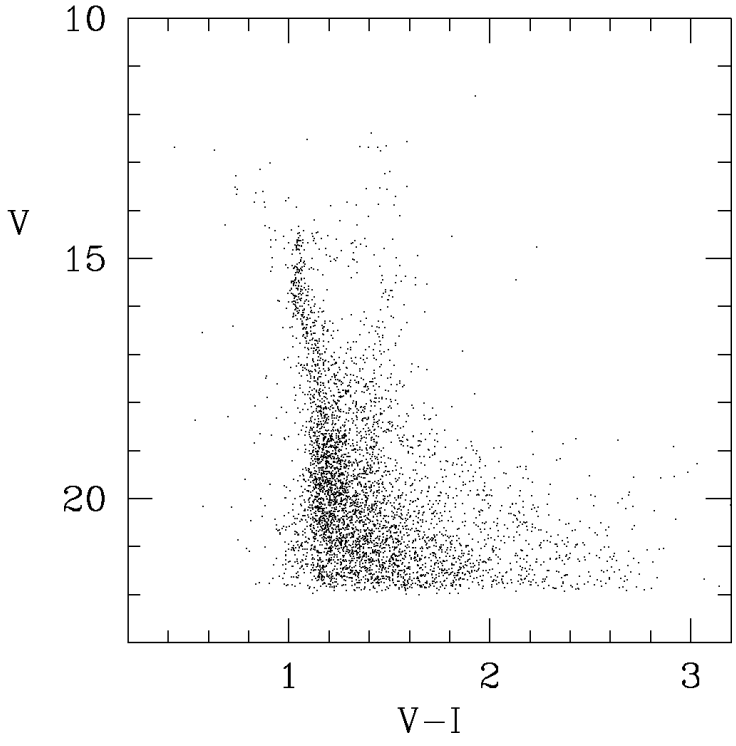
10
15
20
V
1
2
3
V−I

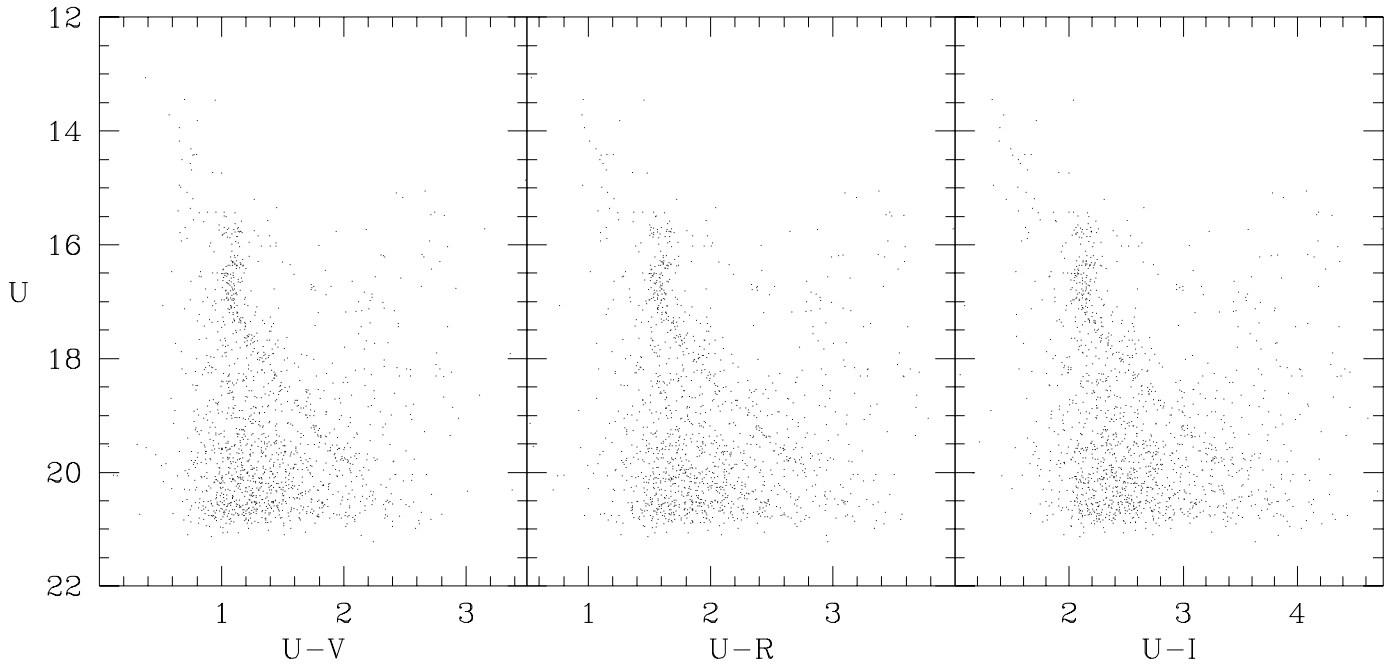
12
14
16
18
20
22
U
1
2
3
U−V
1
2
3
U−R
2
3
4
U−I

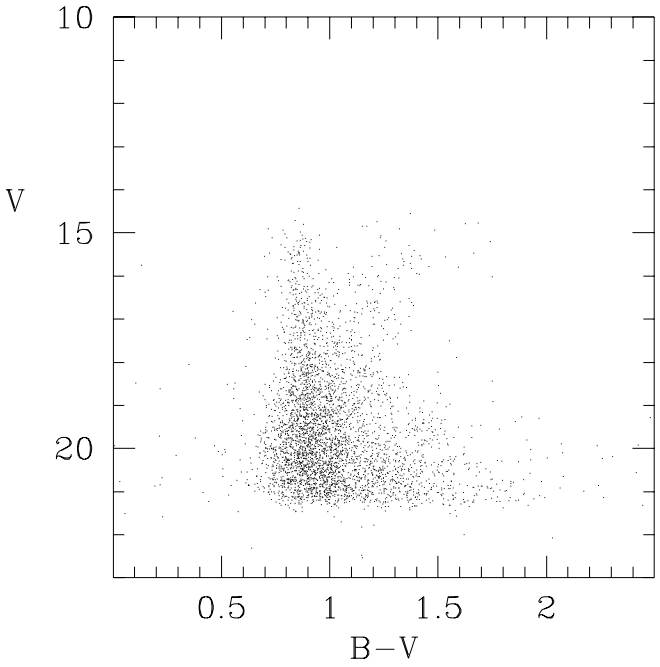
10
15
20
V
0.5
1
1.5
2
B−V

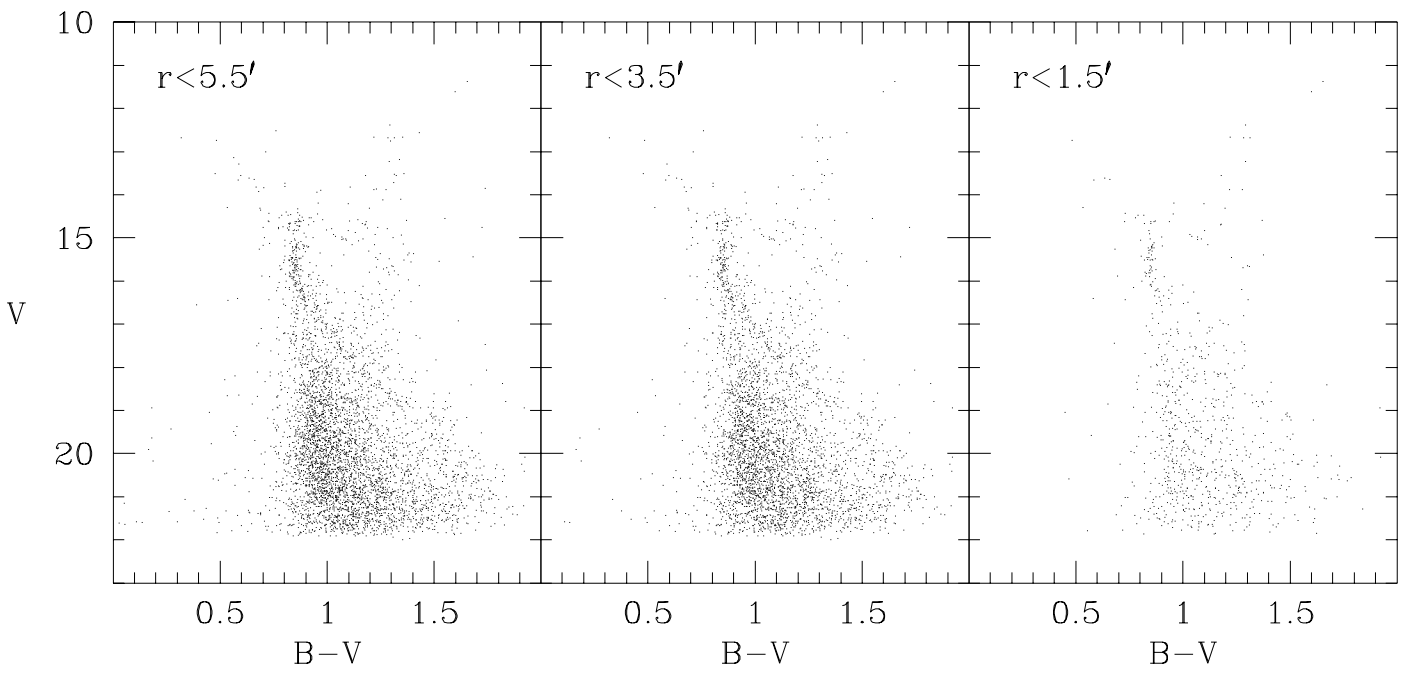
10
15
20
V
r<5.5′
r<3.5′
r<1.5′
0.5
1
1.5
B−V

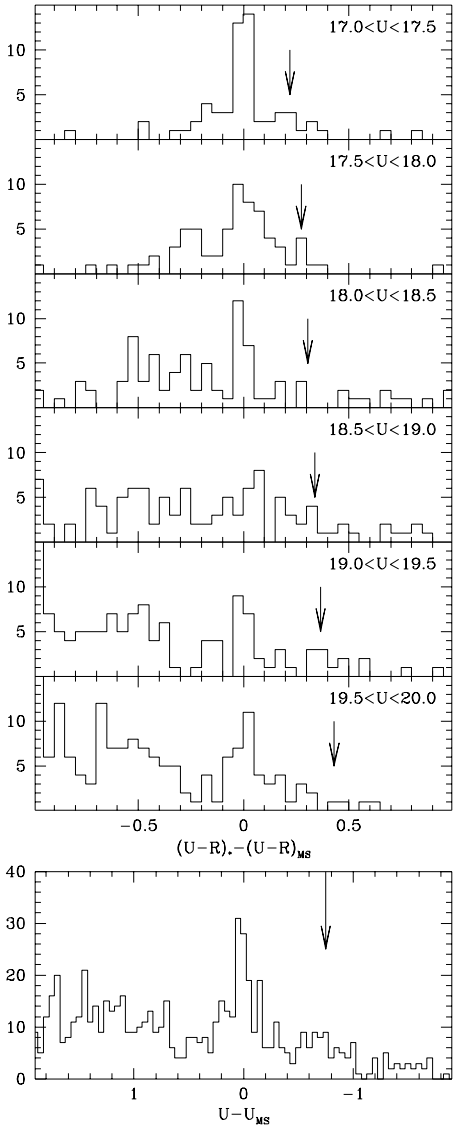
17.0<U<17.5
17.5<U<18.0
18.0<U<18.5
18.5<U<19.0
19.0<U<19.5
19.5<U<20.0
10
5
−0.5
0
0.5
(U−R)*−(U−R)MS
40
30
20
10
0
1
0
−1
U−UMS

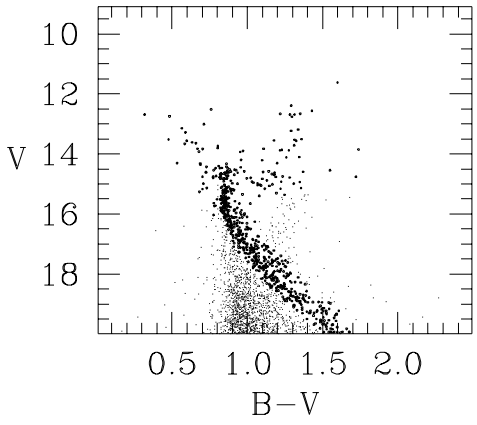
10
12
V 14
16
18
0.5
1.0
1.5
2.0
B−V

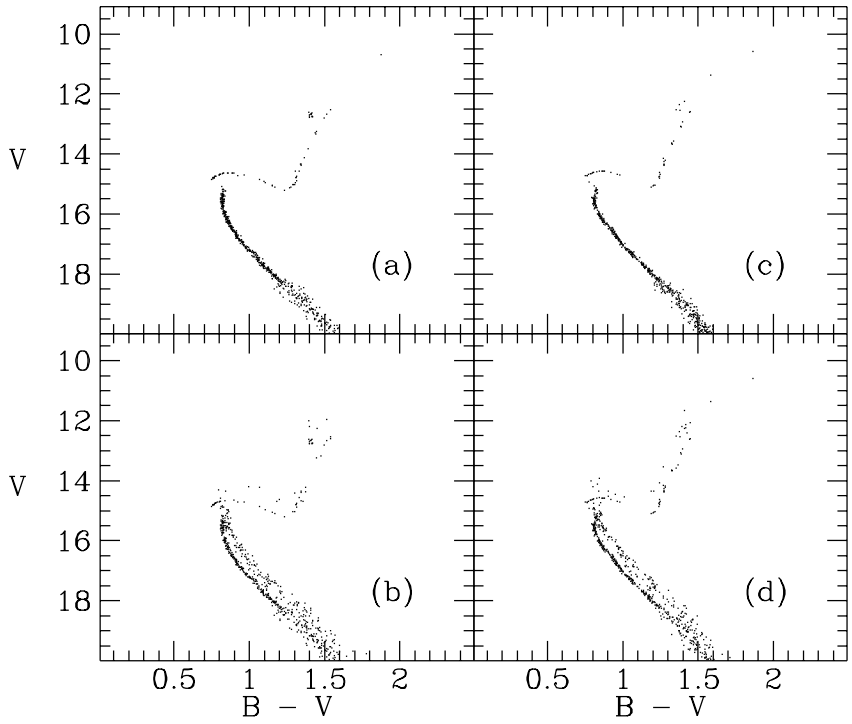
10
12
14
16
18
V
(a)
(c)
(b)
(d)
0.5
1
1.5
2
B − V

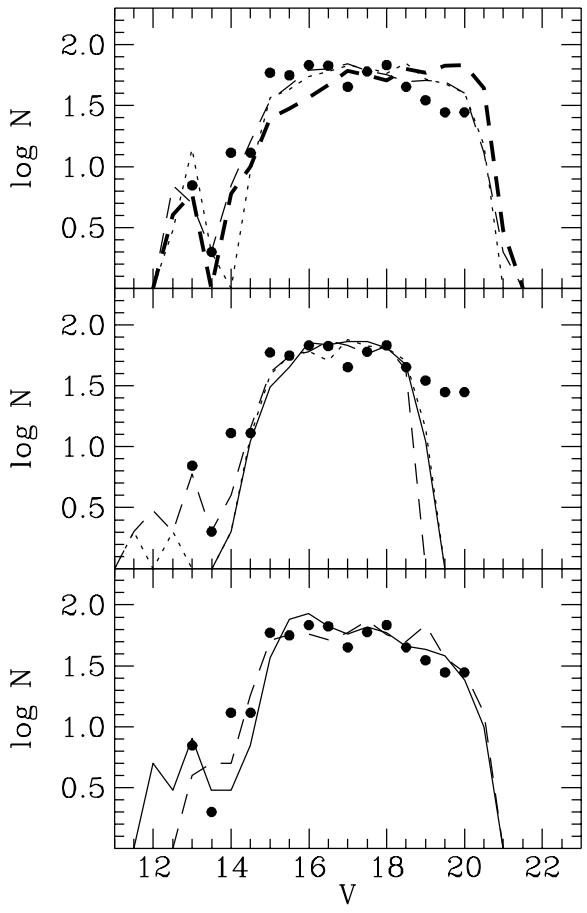
log N
2.0
1.5
1.0
0.5
log N
2.0
1.5
1.0
0.5
log N
2.0
1.5
1.0
0.5
12
14
16
18
20
22
V

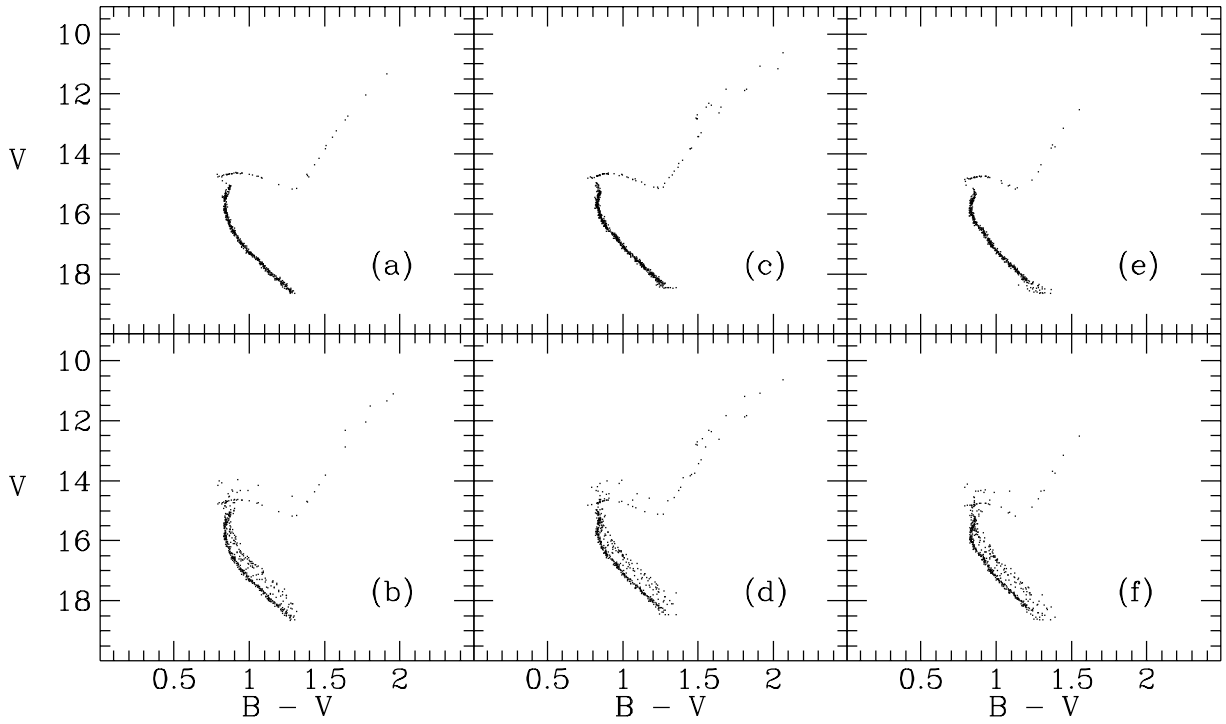
V
10
12
14
16
18
(a)
(c)
(e)
(b)
(d)
(f)
0.5
1
1.5
2
B − V

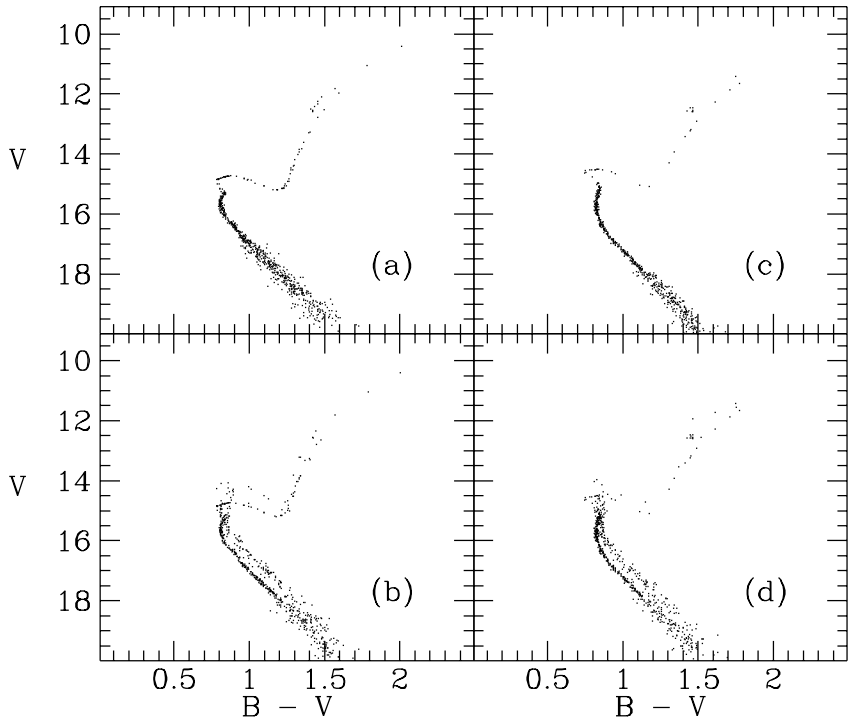
10
12
14
16
18
V
(a)
(c)
(b)
(d)
0.5
1
1.5
2
B − V